

Optimizing Vision Transformers for Medical Image Segmentation and Few-Shot Domain Adaptation

Qianying Liu, Chaitanya Kaul, Christos Anagnostopoulos,
Roderick Murray-Smith, Fani Deligianni
School of Computing Science, University of Glasgow, UK

October 18, 2022

Abstract

Transformers were originally introduced in Natural Language Processing as sequence-to-sequence architectures based on a self-attention mechanism that allows to represent complex relationships in the input data. However, the adaptation of transformers to computer vision is not straightforward because the modelling of image contextual information results in quadratic computational complexity with relation to the input features. Furthermore, most of existing methods require extensive pre-training on massive datasets such as ImageNet and therefore their application to fields such as healthcare is less effective. On the other hand, Convolutional Neural Networks are the dominant architecture in computer vision tasks because convolutional filters can effectively model local dependencies and reduce drastically the parameters required. However, convolutional filters cannot handle more complex interactions, which are beyond a small neighbour of pixels. Furthermore, their weights are fixed after training and thus they do not take into consideration changes in the visual input. Inspired by recent work on hybrid visual transformers with convolutions and hierarchical (Swin) transformers, we propose Convolutional Swin-Unet (CS-Unet) transformer blocks and optimise their settings with relation to patch embedding, projection, the feed-forward network, up sampling and skip connections. CS-Unet can be trained from scratch and inherits the superiority of convolutions in each feature process phase. It helps to encode precise spatial information and produce hierarchical representations that contribute to object concepts at various scales. Experiments show that CS-Unet without pre-training surpasses other state-of-the-art counterparts by large margins on two medical CT and MRI datasets with fewer parameters. In addition, two domain-adaptation experiments on optic disc and polyp image segmentation further prove that our method is highly generalizable and effectively bridges the domain gap between images from different sources.

1 Introduction

Deep convolutional neural networks (convnets) [1] are the most widely used networks for computer vision and they have been quickly adapted for medical image tasks. Unet and its variants [2, 3, 4, 5] with U-shaped structure have prevailed the domain of medical image segmentation and achieved impressive segmentation performance. This is because convolutions enjoy important properties such as sparse interactions, weight sharing, and translation equivariance, giving convnets a strong and useful inductive bias for vision tasks. However, they also suffer from an important intrinsic drawback: they cannot model long-range interactions between pixels due the fixed operation performed on each image sample.

The transformer [6], was designed for sequence modeling in the domain of natural language processing, and has drawn increasing attention from the computer vision community. ViT [7] was the first transformer model adapted into computer vision and outperformed convnets on various downstream vision tasks. Then PVT [8] and Swin transformer [9] proposed a spatial reduction attention and window based attention mechanism respectively to reduce the computational complexity of ViT. CVT [10] and CCT [11] introduced convolutions to transformer block and dispelled the drawback of data hungry of transformer. Some studies [12, 13, 14, 15] exploited transformer in medical image segmentation tasks with promising results but suffered at least one of three major limitations: 1) Most of these methods require large scale pre-training, which is inconvenient and creates computational complexity. 2) Existing transformer blocks or other feature processes still use linear layers which lose important spatial information. 3) Transformer based medical imaging is still in a very early stage and hence, there is no established optimised recipe for their use.

To tackle these problems, we start with a Swin-Unet [14] and combine the well-studied aspects of convolutions with to the most fundamental components of transformer-based architectures (patch embedding, projection, feed-forward network, up sampling and skip connections) to demonstrate how adding spatial context to transformers can potentially boost their performance. By introducing convolutions into the mentioned components, our Convolutional Swin-Unet (CS-Unet) overcomes the shortcomings of transformers (i.e. its data hungry nature and non-local feature modeling) while maintaining their familiar merits (i.e. dynamic attention, global context and better generalization). Experiments on medical CT and MRI datasets show CS-Unet without pre-training surpassed other state-of-the-art methods without pre-training and with fewer parameters while also being highly generalizable demonstrated in its ability to bridge the domain gap between different data sources.

The contributions of our paper are three-folded: (1) We design a Convolutional Swin Transformer (CST) block including convolutional projections for query, key, and value embeddings and a Depthwise separable feed-forward module for spatial feature learning. This makes transformers capable of dealing with long-term interactions while better modelling local information. (2) We proposed CS-Unet for medical image segmentation based on our CST block.

Additionally, a convolutional token embedding is proposed to introduce more spatial information on overlapping token maps. We utilize convolutions to replace typical operation in up-sampling and skip connection which helps fuse multi-scale feature. After adding these modules, position embedding can be safely removed in CS-Unet. (3) Our work sheds valuable insights into creating transformer architectures which can better utilize spatial information in images for feature extraction. We further show that this kind of model generalizes better to small scale medical image datasets compared to state-of-the-art transformer methods with extensive pretraining on ImageNet. At the same time, on two cross-domain segmentation tasks, our CST block outperforms other counterparts consistently in challenging few-shot learning scenarios.

2 Related work

CNN-based models for medical image segmentation: The U-Net [2], which is an encoder-decoder based architecture with skip connections, has been shown to handle high-resolution images with small sample-size well. In medical imaging literature, it is the prevailing architecture for semantic segmentation tasks. Many UNet variants such as U-Net++ [3], Unet 3+ [4], Attn-U-Net [5], FocusNet [16] and FocusNet++ [17] have achieved excellent segmentation results through their ability to incorporate either multi-resolution information, or attention mechanisms (or both) into their feature processing. However, all CNNs including UNet are intrinsically local due to the inherent locality of convolution operations. This restricts their ability to model long-range dependencies within data.

Transformer based models for medical image segmentation: Recently, many works try to solve this problem by using the Transformer architecture. Self-Attention (SA) which is the key component of Transformers, can model long range semantic relations among all input tokens, which gives Transformers the ability to handle long-range dependencies in the data. This helps models become more capable of dealing with non-local interactions. Previous works in the field of medical image segmentation can be divided into two categories depending on their use of either Convolutions or Transformers as a feature processing backbone:

A. Convolution-based stem: TransUNet [12] is the first work to utilize transformers to encode the global context in a CNNs’ feature for medical image segmentation. They kept the familiar U shape of the UNet and used transformer layers followed by convnets as a feature extractor. UNETR [18] use pure transformers as a feature encoder and use a convolutional decoder to obtain a segmentation map, but the entire image processing is on the same scale. It is interesting to note that most convolution-based networks such as TransUNet [12] and their successors (TransFuse [19] and TransAttUnet [13]) that treat CNNs as a backbone, suffer from two major drawbacks. Firstly, they do not leverage the full power of transformers as shallow (one or two transformer blocks) can not encode long-term dependencies present in convolutional representations [20].

Secondly, most of these models have high complexity with far more parameters to train as they stack bulky transformer blocks on top of convolutional feature extractors (which are large pretrained CNN models themselves).

B. Transformer-based stem: To address the above issue, research has moved towards using Transformers as the main stem for building the entire segmentation architectures. MedT [21] proposed a gated axial Transformer layer to build the whole architecture. Karimi et al. [22] removed the convolutional operations from the UNet and built a ViT-like transformer based 3D segmentation model. They divide a 3D image into 3D patches, then flattened them into 1D embedding and fed them into self-attention blocks. Swin-Unet [14] is regarded as the first pure Transformer model for medical image segmentation. It keeps the familiar U-shape of the UNet and adds hierarchical feature extraction using shifted windows proposed by the Swin Transformer [?]. This drastically reduced the quadratic complexity of traditional self-attention. DS-TransUNet [15] followed Swin-Unet and added another encoder pathway to input dual-scale images for performing multi-scale information fusion. MISSFormer [23] followed the pure U-shaped transformer of Swin-Unet but redesigned a new feed-forward module and added Transformer layers in its skip connection. nnFormer [20] modified the embedding, up-sampling and down-sampling with convolutions based on the Swin-Unet. Tragakis et al. [24] presents a fully convolutional transformer structure based on classic multi-head attention module. Wang et al. [25] proposed MT-UNet to model interaction between data points through a local-global attention operation.

Although these architectures have shown promising results, most of them involve large number of parameters, and extensive pre-training on large datasets like ImageNet before they can be fine-tuned to downstream tasks like medical image segmentation. This is sub-optimal due to the lack of large labelled datasets with abnormalities and the prohibitive computational cost. In addition, these works still use linear layers in the transformer block or other feature processes, which misses important spatial information.

Our work aims to alleviate the problems that existing transformers-based segmentation models face. We show via extensive ablation experiments that linear operations inside transformer blocks do not perform well for medical image segmentation tasks. Following this, we identify the optimal settings of incorporating convolutions inside transformers to make them lightweight, efficient, faster and more accurate than existing transformer based models proposed in literature. Our proposed model, CS-Unet, can be trained from scratch and inherits the superiority of convolutions in each feature processing phase. It helps to encode precise spatial information and produce hierarchical representations - something current transformer models lack. Furthermore, we show that the attention mechanisms in transformers and convolutions are in fact highly complementary in nature, and shed valuable insights into creating architectures that can optimally fuse spatial information from medical images.

3 Method

3.1 Overall Structure Design

The overall architecture of the proposed Convolutional Swin-UNet(CS-UNet) is presented in Figure 1. The encoder of the model comprises of one embedding layer, three CST layers, each layer contains two successive window and shift window blocks, (as shown in stage 1) and three patch merging layers. The patches are sent to the bottleneck which contains two CST blocks. We design a symmetrical decoder which includes three CST layers, three up-sampling layers and one patch expanding layer to perform 4x up-sampling. Skip connections are added between corresponding feature pyramids of the encoder and decoder. Skip convolutions further fuse the multi-scale features and help to recover fine-grained information lost in down-sampling.

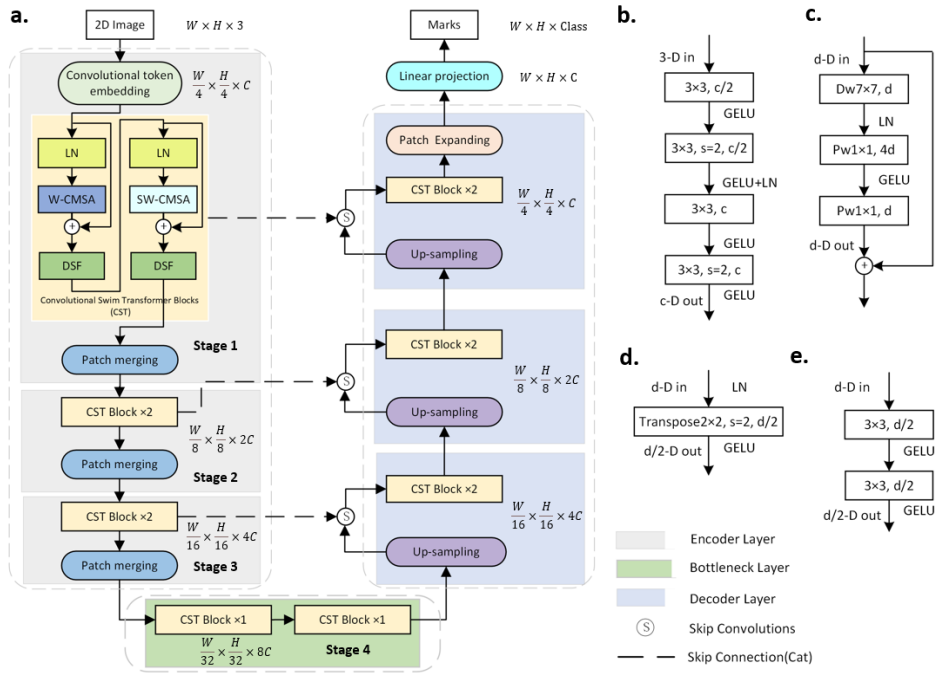


Figure 1: (a) Overall architecture of CS-UNet. Encoder, bottleneck and decoder consist of three, one and three CST layers, respectively, (b) convolutional token embedding, (c) DSF, (d) upsampling mechanisms and (e) skip convolutions. D is the number of channels of feature. d is the current number of channels, c is an arbitrary dimension.

3.2 Convolutional Swin Transformer Block (CST)

Our CST block is based on a swin transformer block [14] which introduces shifted windows to transformer projections to reduce complexity and integrate locality. We revise this block by i) replacing the linear projections in self-attention modules with convolutional projections for query, key, and value embeddings and ii) replacing the MLP with a depthwise separable feed-forward (DSF) module. Both these changes improve model accuracy while reducing the number of parameters.

In stage 1 of Figure 1 (a), two consecutive CST blocks are presented. The window based convolutional multi-head self attention (W-CMSA) module and shifted window based convolutional multi-head self attention (SW-CMSA) module are applied in the two successive CST blocks, respectively. In Figure 2, we show the details of the first CST block for brevity. Each block is composed of Layer Norm (LN) layer, W-CMSA module, residual connection (RC) and 3-layer DSF module with GELU activation. When the features are input into next CST block, a shifted window partition is applied to change the attention area.

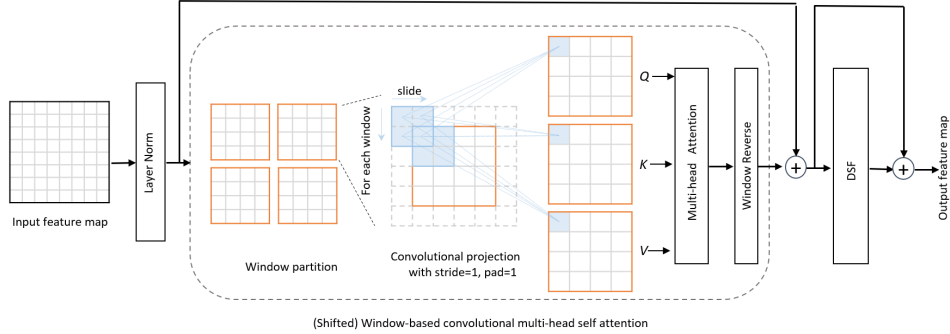


Figure 2: Convolutional Swin Transformer (CST) Block.

(Shifted) Window based convolutional multi-head self attention

As shown in Figure 2, once tokens enter (S)W-CMSA, they are reshaped into a 2D token map, and partitioned into windows. For each window, we use three Depth-wise convolutions with kernel size of 3×3 , pad of 1 and stride of 1 to create our Q , K and V projection matrices. The three matrices are then flattened into token vectors following which we compute the multi-head self-attention via Eq.(1):

$$Attention(Q, K, V) = SoftMax\left(\frac{QK^T}{\sqrt{d}} + B\right) V \quad (1)$$

Here Q , K , V are the query, key and value matrices, respectively. d represents the dimension of the query or key. The values in B are from the bias. We feed

the attention into a 3×3 Depth-wise convolution for fine-tuning. We follow this by reversing the windows to 2D token maps, resulting in more robust estimations than the standard swin transformer [9] as it removes our dependence on having a positional encoding in our model.

Instead of position-wise linear projections used in conventional Transformer based Unets, (S)W-CMSA achieves better modeling of local spatial context resulting in a more efficient architecture. This module is inspired by [10]. Our work however, is different from [10] as we conduct projection based on windows rather than the whole image, leading to more refined local features as the kernels learnt on each window are different. In order to better adapt to medical images with smaller data volumes, Point-wise convolutions are removed to avoid over-fitting. Furthermore, the Batch Normalization layer is changed to LN layer as it achieves better performance.

Depthwise separable feed-forward (DSF) module After computing the (S)W-CMSA, the feature maps are fed into a feed-forward module. Transformers implement this module as an MLP: $\text{LN}, d \rightarrow \text{Linear}, 4 \times d \rightarrow \text{GELU} \rightarrow \text{Linear}, d \rightarrow \text{RC}$. The d denotes the number of channels of a reshaped feature map. We propose a DSF module as a choice of feed-forward module which provides the model spatial context. We use three Depth-wise convolution operations instead of two linear layers for reducing the number of parameters and utilizing the features between channels. In addition, we found that LN at later layer can lead to better segmentation results. The DSF is implemented as: $7 \times 7 \text{ Depth-wise Conv}, d \rightarrow \text{LN}, d \rightarrow \text{Point-wise Conv}, 4 \times d \rightarrow \text{GELU} \rightarrow \text{Point-wise Conv}, d \rightarrow \text{RC}$.

3.3 Encoder

The input of our model is a 2D slice with the resolution of $H \times W \times 3$ sampled from a 3D volume of images. H , W and 3 denote the height, width and number of channels of each input. The input image is passed through the convolutional token embedding layer to create a sequence embedding with the resolution of $\frac{H}{4} \times \frac{W}{4} \times C$ ($C = 96$ in later experiments). These embeddings are fed into three main layers. Each layer includes two CST blocks and a patch merging module which downsamples the image and doubles the number of channels. For example, the first patch merging module, the input with $\frac{H}{4} \times \frac{W}{4} \times C$ are divided into four parts and concatenated along the C dimension to create a feature map with $\frac{H}{8} \times \frac{W}{8} \times 4C$. Then a linear layer is applied to this map to $2 \times$ reduce the C dimension.

Convolutional Token Embedding layer Existing models using shifted windows split images into non-overlapping patches and increase dimensionality using a linear layer. Our embedding layer however, is implemented as four convolutions with overlapping patches and outputs 2D reshaped token maps with C dimension directly. This overlapping process helps introduce more spatial information. Then the token maps with resolution $\frac{H}{4} \times \frac{W}{4} \times C$ are flattened into $\frac{H}{4} \times \frac{W}{4} \times C$. Specifically, this module is implemented as follows: $3 \times 3 \text{ s}=1 \text{ Conv}, d/2 \rightarrow \text{GELU} \rightarrow 3 \times 3 \text{ s}=2 \text{ Conv}, d/2 \rightarrow \text{GELU} + \text{LN} \rightarrow 3 \times 3 \text{ s}=1 \text{ Conv}, d \rightarrow$

GELU \rightarrow 3×3 $s=2$ Conv, $d \rightarrow$ GELU. Here, s is stride and the dimension of input is 3, and $d = C$.

Bottleneck The bottleneck has two successive CST blocks, and both of them are based on W-CMSA. During this period the size of feature map remains unchanged.

3.4 Decoder

A symmetric decoder is built corresponding to the encoder. We use strided deconvolution to $2 \times$ up-sample feature maps and halve the feature dimension. The convolutional up-sampling is implemented as : LN, $d \rightarrow 2 \times 2$ $s=2$ ConvTranspose, $d/2 \rightarrow$ GELU. The output of high-resolution feature maps are concatenated with shallow feature representations from the encoder, and then merged through skip convolutions module to better capture both spatial and fine-grained information. The skip convolutions module is implemented as : 3×3 $s=1$ Conv, $d/2 \rightarrow$ GELU $\rightarrow 3 \times 3$ $s=1$ Conv, $d/2 \rightarrow$ GELU. Although methods like [14] only adopts a linear layer for merging the skip connection from the encoder, our experiments showed that this is not enough to reduce the information lost by downsampling.

After repeating the above process three times, the features are fed into the patch expansion layer. This involves $4 \times$ up-sampling followed by a linear projection to fine tune the final segmentation prediction. This is similar to [?], as we find that patch expansion obtains a high accuracy in the final segmentation stage.

4 Experiments

4.1 Datasets

We use two publicly available datasets to benchmark our proposed architecture.

Synapse multiorgan segmentation (Synapse): This dataset contains abdominal CT scans from 30 subjects. Following [12], 18 cases (2212 axial slices) are extracted for training, while other 12 cases are used for testing. We report the model performance evaluated with the average Dice score (DSC) and average Hausdorff Distance (HD) on eight abdominal organs, which are aorta, gallbladder, spleen, left kidney, right kidney, liver, pancreas and stomach.

Automatic Cardiac Diagnosis Challenge (ACDC): ACDC contains MRI images from 100 patients, with the cavity of the right ventricle, the myocardium of the left ventricle and the cavity of the left ventricle to be segmented. The dataset is split (as in [25]) into 70 (1930 axial slices), 10 and 20 for training, validation and testing, respectively. The evaluation metrics used are the average Dice Coefficient (DSC) and Hausdorff Distance (HD).

4.2 Implementation details

Our experiment setting is similar to [12] and [14]. We compare our performance with three categories of models, including pure CNN-based models (R50 U-Net and R50 Att-U-Net), hybrid transformer-based models (R50 ViT, TransUnet), and a pure transformer-based model, (Swin-Unet). We keep the same experimental set up as our baseline model (optimizer, number of epochs and the structure of encoder), Swin-Unet. We train our models on Python 3.8 and Pytorch 1.7.1 using a single Nvidia RTX3090 GPU with 24GB memory. For all the experiments, simple data augmentations including flipping and rotations were used on all the training data to increase the robustness. The input image size is 224×224 . Pre-trained weights are used for other methods if provided, while our model is trained from scratch. Our model was trained for 300 epochs for the two datasets and the parameters were randomly initialized. During the training period, the batch size is 24 and a combination of the cross entropy and dice loss is used. In addition, we use an AdamW optimizer with a weight decay of $5E-4$ for both datasets. The learning rates for Synapse and ACDC are $1e-3$ and $5e-3$, respectively. We start with a 10-epoch linear warmup. Layer Scale [26] of initial value $1e-6$ is applied.

5 Results

5.1 Results on Synapse dataset

As shown in Table 5.1, we compare our model with a variety of convolution-based and transformer-based approaches on Synapse. The results demonstrate that CS-Unet achieves the best DSC of 82.21% and outperforms SwinUnet and MT-UNet by 3.08 and 3.62 percents respectively, as well as a HD score competitive with state-of-the-art models. Our method gets the highest DSC for five organs, especially for challenging cases like the gallbladder and pancreas. CS-Unet contains 24 million parameters making it smaller than SwimUnet (27 million) and TransUnet (96 million).

Figure 3 show the segmentation results of our method, MT-UNet and SwinUnet. The over-segmentation problems are clearly observed on MT-UNet and SwinUnet on stomach and liver. In addition our method better delineates the pancreas in case 1 and 2.

5.2 Results on ACDC dataset

Table 5.2 shows our performance on the ACDC dataset. We can see that our method achieves best average DSC and best DSC on RV and Myo. In addition, we surpass SwinUnet by 3.3% in average DSC and in all classes. Our results prove that combining convolutions and self-attention can improve the capability of medical image semantic segmentation.

Figure 4 shows the visualization of segmentation results of three methods. Our CS-Unet is more discriminative than other models in nearly all cases.

Methods	DSC(%)	HD(mm)	Aorta	Gallbladder	Kidney(L)	Kidney(R)	Liver	Pancreas	Spleen	Stomach
R50 U-Net [12]	74.68	36.87	84.18	62.84	79.19	71.29	93.35	48.23	84.41	73.92
R50 Att-U-Net [12]	75.57	36.97	55.92	63.91	79.20	72.71	93.56	49.37	87.19	74.95
UNet [2]	76.85	39.70	89.07	69.72	77.77	68.60	93.43	53.98	86.67	75.58
AttnUNet [5]	77.77	36.02	89.55	68.88	77.98	71.11	93.57	58.04	87.30	75.75
R50 ViT [12]	71.29	32.87	73.73	55.13	75.80	72.20	91.51	45.99	81.99	73.95
TransUnet [12]	77.48	31.69	87.23	63.13	81.87	77.02	94.08	55.86	85.08	75.62
SwinUnet [14]	79.13	21.55	85.47	66.53	83.28	79.61	94.29	56.58	90.66	76.60
MT-UNet [25]	78.59	26.59	87.92	64.99	81.47	77.29	93.06	59.46	87.75	76.81
Ours	82.21	27.02	88.40	72.59	85.28	79.52	94.35	70.12	91.06	75.72

Table 1: Comparison with different models on multi-organ segmentation (Synapse)

Specifically, CS-Unet greatly reduces the number of false positive predictions (cases 1 and 2), while also capturing the shape of RV better than MT-UNet in case 3.

Methods	DSC(%)	RV	Myo	LV
R50 U-Net [12]	87.60	84.62	84.52	93.68
R50 Att-U-Net [12]	86.90	83.27	84.33	93.53
R50 ViT [12]	86.19	82.51	83.01	93.05
TransUnet [12]	89.71	86.67	87.27	95.18
SwinUnet [14]	88.07	85.77	84.42	94.03
MT-UNet [25]	90.43	86.64	89.04	95.62
Ours	91.37	89.20	89.47	95.42

Table 2: Comparison with different models on cardiac segmentation (ACDC)

5.3 Ablation study

In order to explore the influence of our modules on the model performance, we conducted experiments on both of ACDC and Synapse used DSC and HD as evaluation metric. The results are shown in Table 3. The original Swin-Unet using optimizer of AdamW and SGD trained from scratch are treated as the baseline for these experiments.

For method 0 (adding convolutional embeddings), we observe large improvements of 17% and 8% on ACDC and Synapse respectively. By further adding just convolutional projections, the segmentation results are very close to Swin-Unet used pre-trained Imagenet weight emphasizing the importance of convolution based transformers. Surprisingly (method 2), removing the position embedding in early stage leads to a slight drop in performance. This is because spatial context is lost in the MLP based feedforward layer of the current architecture. We confirm this through experiments in methods 7,9,8 and 10, where the models are all fully convolutional, proving that convolution based transformers can track the position of pixels better than positional embedding, and that

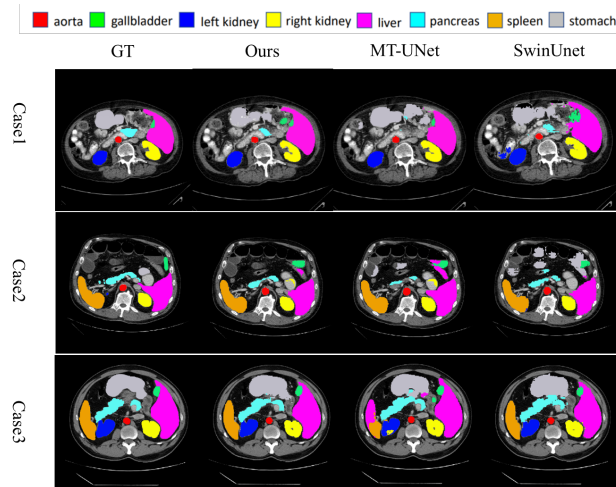


Figure 3: Visualization of segmentation results on the Synapse dataset. Our method is compared with Ground Truth, MT-UNet and SwinUnet.

spatial feature extraction, is in fact, a necessity for transformer based architectures. We systematically added convolutional layers to finetune the attention computation (method 3 onwards), and DSF modules (method 5 onwards) and observed a good boost in both datasets’ performance. Our experiments with the deconvolution and skip convolutions are used to upsample features in the network decoder. A degeneracy of 0.17 percents can be found on DSC of ACDC, but 2.56 improvements of the overall performance on DSC of Synapse. It demonstrates that the deconvolution and skip convolution may be a good alternative choice when we design up-sampling and skip connection of transformer-based networks. Methods 4, 6, 8 and 10 replace convolutions in the immediately preceding method with depthwise convolutions (for processing the CMSA output) to observe their effects on feature processing. Overall, (as seen from Table 3), adding depthwise convolutions tend to create more accurate and robust transformers for segmentation while keeping the number of parameters low. Our best performing model (model 10) gets significantly higher dice scores on both ACDC and Synapse datasets with fewer parameters than the Swin-Unet.

In addition, we explore the effect of different convolutional feed-forward modules on our model. Our results are summarized in Table 4. Single convolution refers to a 3x3 convolution layer with layer normalization instead of batch normalization. Our experiment here showed that LN helps achieve better results than BN in transformers.

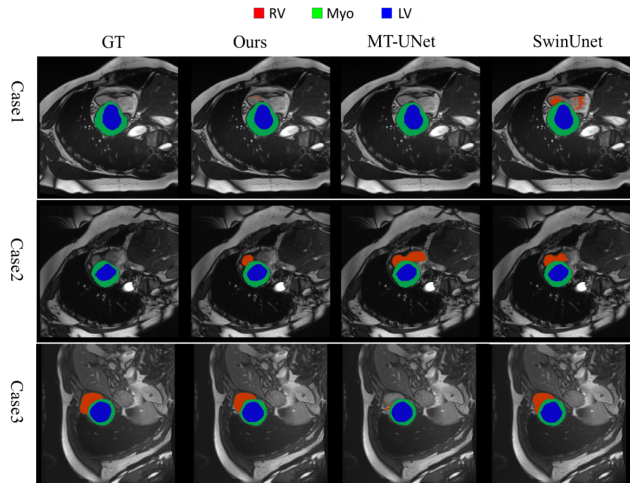


Figure 4: Visualization of segmentation results on the ACDC dataset.

5.4 CST block in few-shot domain adaptation

For medical image segmentation, deep neural networks (DNNs) trained on one set of medical images still face an issue of Domain Adaptation(DA), i.e. severe performance drop on unseen test images in the presence of even small distribution shifts in the test set. Models are expected to generalize well to such distribution and domain shifts, for instance, models trained on images acquired from one sensor should ideally work for image captured with different devices. One option to achieve this is the brute force approach of collecting large annotated target domain data. However, this is not generally possible in clinical scenarios, where data acquisition and labeling are very expensive in terms of cost and time. Few-shot domain adaptation, i.e., adapting a trained model with a handful of annotations, hence serves as a highly practical option to fill the various domain discrepancies between the training images (source domain) and the test images (target domain). In this section, we show how our proposed transformer block can be used to enhance few-shot domain adaptation.

Firstly, we train CST on the source domain in order to extract a set of source-domain embeddings. Subsequently, we let the CST layer adapt to the target domain by only updating a projection layer of K in the self-attention module, and thus fitting a few annotated images well.

We compare our model with the Polymorphic Transformer (Polyformer) [30] as it is the state-of-the-art in domain adaptation for medical image segmentation. We keep the setting proposed in [30] with the notable exception that we replace the Polyformer with our CST block. Figure 5 shows our proposed set up.

Our results show that CST outperforms the Polyformer with two major

Methods	ACDC		Synapse		C_Emb	C_Proj	No_Pos	C_Att	DSF	C_Up+C_sk	#params (M)
	DSC	HD	DSC	HD							
SwinUet(AdamW)	68.87	10.90	60.80	54.35							27
SwinUet(SGD)	82.51	3.53	66.30	34.05							27
0	85.94	3.67	68.57	51.02	✓						21
1	90.86	1.69	77.47	18.54	✓	✓					21
2	89.45	2.25	78.31	25.58	✓	✓	✓				21
3	90.57	1.50	78.43	27.09	✓	✓	✓	<i>C</i>			37
4	89.89	2.98	78.32	25.43	✓	✓	✓	<i>D.C</i>			19
5	91.43	1.28	78.52	25.30	✓	✓	✓	<i>C</i>	✓		37
6	91.30	1.35	79.04	22.96	✓	✓	✓	<i>D.C</i>	✓		19
7	91.07	1.74	80.74	29.24	✓	✓		<i>C</i>	✓	✓	42
8	91.30	2.00	81.93	24.59	✓	✓		<i>D.C</i>	✓	✓	24
9	91.26	1.80	81.08	26.07	✓	✓	✓	<i>C</i>	✓	✓	42
10	91.37	2.04	82.21	27.02	✓	✓	✓	<i>D.C</i>	✓	✓	24

Table 3: Ablation study on the impact of different modules used in CS-Unet. C_Emb represents convolutional token embedding, C_Proj denotes Depth-wise convolutional projection in attention module, No_Pos means position embedding is removed in transformer block, C_Att means we use a convolution layer to fine tune the attention at the end of CMSA (*D.C* and *C* present Depth-wise and spatial convolution respectively), DSF denotes MLP is replaced by DSF module and C_Up+C_sk indicates deconvolution and skip convolution are used for up-sampling and skip connection.

Methods	DSC	HD	Aorta	Gallbladder	Kidney(L)	Kidney(R)	Liver	Pancreas	Spleen	Stomach
Single convolution	79.66	27.67	88.50	67.89	83.62	79.75	92.54	64.31	87.74	72.93
Residual block [27]	79.13	28.85	87.61	70.23	80.28	71.54	94.18	63.36	89.70	76.17
Pre-act residual block [28]	78.19	28.86	87.09	65.36	80.90	74.91	93.52	60.83	88.17	74.72
ResNeXt block [29]	78.93	30.87	87.30	68.69	81.10	75.17	93.37	61.06	89.94	74.83
Ours	82.21	27.02	88.40	72.59	85.28	79.52	94.35	70.12	91.06	75.72

Table 4: Ablation study on the impact of different feed forward modules

advantages: (1). Unlike the Polyformer, we do not input any extra embeddings (called prototypes, which increase computational overhead) into our set up. This helps us reduce the feature space of the attention matrix in multi-head attention computation. As CST uses window mechanism to reduce computation load, it is simpler, and also better at learning the feature on the non-compressed input. (2). Our convolutional operation including projection and DSF helps utilize local feature learning than ordinary multi-head attention.

Similarly to [30], we test our approach on two medical segmentation tasks: (1) *Optic disc/cup segmentation*: This task is based on 2D images of the rear of the eyes. The REFUGE challenge [31] provides 1200 training images for source domain. And we adopts 159 images from the RIM-One dataset [32] for the target domain. (2) *Polyp segmentation*: This task segments polyps in 2D colonoscopy images. The source domain includes CVC-612 [33] and Kvasir [34] which have 612 and 1000 images respectively. While just 60 images of CVC-

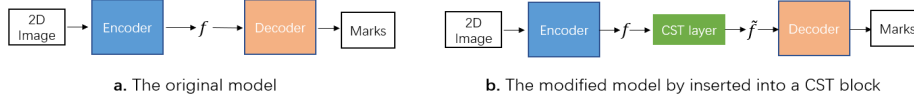


Figure 5: The original model consists of an encoder and a decoder (a). (b) shows a modified model for domain adaptation with an inserted CST. The transformer layer converts features f to \tilde{f} . While the weights of the encoder and decoder are frozen.

300 dataset [35] are used for target domain. For simplicity, we keep the same setting as [30] in terms of the number of epochs, the optimizer and total number of parameters in our model. It is useful to note that this actually places CST at a disadvantage, as we do not conduct any extra hyper-parameter search to make our model more robust. Even then, CST surpasses the performance of the Polyformer.

Methods	RIM-One		CVC-300	Avg.
	Disc	Cup		
U-Net(source) [2]	81.9	70.8	72.8	75.2
U-Net(\mathcal{L}_{sup}) [2]	87.1	66.5	79.1	77.6
RevGrad ($\mathcal{L}_{sup} + \mathcal{L}_{adv}$) [36]	86.0	73.2	81.3	80.2
ADDA($\mathcal{L}_{sup} + \mathcal{L}_{adv}$) [37]	87.4	72.6	83.6	81.2
DA-ADV (tune whole model) [38, 39]	88.5	72.5	83.0	81.3
Polyformer($\mathcal{L}_{sup} + \mathcal{L}_{adv} + K$) [30]	91.3	75.8	83.4	83.5
Swinformer($\mathcal{L}_{sup} + \mathcal{L}_{adv} + K$) [9]	91.1	78.2	85.4	85.4
CST($\mathcal{L}_{sup} + \mathcal{L}_{adv} + K$)	92.1	79.3	85.7	85.7

Table 5: Dice scores (%) on Fundus and Polyp target domains RIM-One and CVC-300.

Results are shown in Table 5 where we extend the table proposed in [30] with results of the Swin transformer [9] and our CST model. We choose the U-Net as our backbone. The U-Net without any domain adaptation is used as baseline. Our method along with five DA methods are evaluated. We use two traditional domain adversarial losses: \mathcal{L}_{sup} (few-shot supervision on five images) [36] and \mathcal{L}_{adv} (domain adversarial learning) [37] which are standard for this task. The K in this case refers to fine-tuning the K projection via the above losses. It can be clearly seen that our method achieves the highest average dice scores on RIM and CVC-300 datasets among all the methods. In particular, it is about 4% higher than Polyformer on the CUP segmentation tasks and over 2% higher than the Polyformer for the poly segmentation task. Notably, our method also outperforms the Swin UNet on both tasks. This shows that our CST block effectively reduced domain discrepancy between the source and target domains better than the state-of-the-art Polyformer model specifically proposed for this task, without any pretraining or hyperparameter tuning.

6 Conclusions

We leverage the power of convolutions and transformer architectures for image segmentation and few-shot domain adaptation. Our proposed CST block introduces convolutions in projection and FFN, and it also combines convolutions with token embedding, up-sampling and skip connection to exploit spatial information of images through fusing features across multiple scales. Our experiments show that by replacing linear layers with convolutions we improve the performance of the model drastically across CT and MRI datasets. Our proposed model obtains an average Dice score of 82.21 on the Synapse test set and 91.37 on ACDC, showing significant improvement in performance compared to classical transformer-based methods. In addition, our results show that introducing convolutional components in transformer can leverage better spatial context from images and locate the position of pixels accurately. This means that the positional encoding can be removed from the architecture, making it simpler. Finally, we applied our CST block on domain adaptation to demonstrate its generalization ability in a few shot learning setting.

References

- [1] LeCun, Y., Bottou, L., Bengio, Y., Haffner, P.: Gradient-based learning applied to document recognition. *Proceedings of the IEEE* **86** (1998) 2278–2324
- [2] Ronneberger, O., Fischer, P., Brox, T.: U-net: Convolutional networks for biomedical image segmentation. In: *International Conference on Medical image computing and computer-assisted intervention*, Springer (2015) 234–241
- [3] Zhou, Z., Rahman Siddiquee, M.M., Tajbakhsh, N., Liang, J.: Unet++: A nested u-net architecture for medical image segmentation. In: *Deep learning in medical image analysis and multimodal learning for clinical decision support*. Springer (2018) 3–11
- [4] Huang, H., Lin, L., Tong, R., Hu, H., Zhang, Q., Iwamoto, Y., Han, X., Chen, Y.W., Wu, J.: Unet 3+: A full-scale connected unet for medical image segmentation. In: *ICASSP 2020-2020 IEEE International Conference on Acoustics, Speech and Signal Processing (ICASSP), IEEE* (2020) 1055–1059
- [5] Schlemper, J., Oktay, O., Schaap, M., Heinrich, M., Kainz, B., Glocker, B., Rueckert, D.: Attention gated networks: Learning to leverage salient regions in medical images. *Medical image analysis* **53** (2019) 197–207
- [6] Vaswani, A., Shazeer, N., Parmar, N., Uszkoreit, J., Jones, L., Gomez, A.N., Kaiser, L., Polosukhin, I.: Attention is all you need. *Advances in neural information processing systems* **30** (2017)

- [7] Dosovitskiy, A., Beyer, L., Kolesnikov, A., Weissenborn, D., Zhai, X., Unterthiner, T., Dehghani, M., Minderer, M., Heigold, G., Gelly, S., et al.: An image is worth 16x16 words: Transformers for image recognition at scale. arXiv preprint arXiv:2010.11929 (2020)
- [8] Wang, W., Xie, E., Li, X., Fan, D.P., Song, K., Liang, D., Lu, T., Luo, P., Shao, L.: Pyramid vision transformer: A versatile backbone for dense prediction without convolutions. In: Proceedings of the IEEE/CVF International Conference on Computer Vision. (2021) 568–578
- [9] Liu, Z., Lin, Y., Cao, Y., Hu, H., Wei, Y., Zhang, Z., Lin, S., Guo, B.: Swin transformer: Hierarchical vision transformer using shifted windows. In: Proceedings of the IEEE/CVF International Conference on Computer Vision. (2021) 10012–10022
- [10] Wu, H., Xiao, B., Codella, N., Liu, M., Dai, X., Yuan, L., Zhang, L.: Cvt: Introducing convolutions to vision transformers. In: Proceedings of the IEEE/CVF International Conference on Computer Vision. (2021) 22–31
- [11] Hassani, A., Walton, S., Shah, N., Abuduweili, A., Li, J., Shi, H.: Escaping the big data paradigm with compact transformers. arXiv preprint arXiv:2104.05704 (2021)
- [12] Chen, J., Lu, Y., Yu, Q., Luo, X., Adeli, E., Wang, Y., Lu, L., Yuille, A.L., Zhou, Y.: Transunet: Transformers make strong encoders for medical image segmentation. arXiv preprint arXiv:2102.04306 (2021)
- [13] Chen, B., Liu, Y., Zhang, Z., Lu, G., Zhang, D.: Transattunet: Multi-level attention-guided u-net with transformer for medical image segmentation. arXiv preprint arXiv:2107.05274 (2021)
- [14] Cao, H., Wang, Y., Chen, J., Jiang, D., Zhang, X., Tian, Q., Wang, M.: Swin-unet: Unet-like pure transformer for medical image segmentation. arXiv preprint arXiv:2105.05537 (2021)
- [15] Lin, A., Chen, B., Xu, J., Zhang, Z., Lu, G., Zhang, D.: Ds-transunet: Dual swin transformer u-net for medical image segmentation. IEEE Transactions on Instrumentation and Measurement (2022)
- [16] Kaul, C., Manandhar, S., Pears, N.: Focusnet: An attention-based fully convolutional network for medical image segmentation. In: 2019 IEEE 16th international symposium on biomedical imaging (ISBI 2019), IEEE (2019) 455–458
- [17] Kaul, C., Pears, N., Dai, H., Murray-Smith, R., Manandhar, S.: Focusnet++: Attentive aggregated transformations for efficient and accurate medical image segmentation. In: 2021 IEEE 18th International Symposium on Biomedical Imaging (ISBI), IEEE (2021) 1042–1046

- [18] Hatamizadeh, A., Tang, Y., Nath, V., Yang, D., Myronenko, A., Landman, B., Roth, H.R., Xu, D.: Unetr: Transformers for 3d medical image segmentation. In: Proceedings of the IEEE/CVF Winter Conference on Applications of Computer Vision. (2022) 574–584
- [19] Zhang, Y., Liu, H., Hu, Q.: Transfuse: Fusing transformers and cnns for medical image segmentation. In: International Conference on Medical Image Computing and Computer-Assisted Intervention, Springer (2021) 14–24
- [20] Zhou, H.Y., Guo, J., Zhang, Y., Yu, L., Wang, L., Yu, Y.: nnformer: Interleaved transformer for volumetric segmentation. arXiv preprint arXiv:2109.03201 (2021)
- [21] Valanarasu, J.M.J., Oza, P., Hacihaliloglu, I., Patel, V.M.: Medical transformer: Gated axial-attention for medical image segmentation. In: International Conference on Medical Image Computing and Computer-Assisted Intervention, Springer (2021) 36–46
- [22] Karimi, D., Vasylechko, S.D., Gholipour, A.: Convolution-free medical image segmentation using transformers. In: International Conference on Medical Image Computing and Computer-Assisted Intervention, Springer (2021) 78–88
- [23] Huang, X., Deng, Z., Li, D., Yuan, X.: Missformer: An effective medical image segmentation transformer. arXiv preprint arXiv:2109.07162 (2021)
- [24] Tragakis, A., Kaul, C., Murray-Smith Roderick, H.D.: The fully convolutional transformer for medical image segmentation. In: <https://arxiv.org/abs/2206.00566>. (2022)
- [25] Wang, H., Xie, S., Lin, L., Iwamoto, Y., Han, X.H., Chen, Y.W., Tong, R.: Mixed transformer u-net for medical image segmentation. In: ICASSP 2022-2022 IEEE International Conference on Acoustics, Speech and Signal Processing (ICASSP), IEEE (2022) 2390–2394
- [26] Touvron, H., Cord, M., Sablayrolles, A., Synnaeve, G., Jégou, H.: Going deeper with image transformers. In: Proceedings of the IEEE/CVF International Conference on Computer Vision. (2021) 32–42
- [27] He, K., Zhang, X., Ren, S., Sun, J.: Deep residual learning for image recognition. In: Proceedings of the IEEE conference on computer vision and pattern recognition. (2016) 770–778
- [28] He, K., Zhang, X., Ren, S., Sun, J.: Identity mappings in deep residual networks. In: European conference on computer vision, Springer (2016) 630–645

- [29] Xie, S., Girshick, R., Dollár, P., Tu, Z., He, K.: Aggregated residual transformations for deep neural networks. In: Proceedings of the IEEE conference on computer vision and pattern recognition. (2017) 1492–1500
- [30] Li, S., Sui, X., Fu, J., Fu, H., Luo, X., Feng, Y., Xu, X., Liu, Y., Ting, D.S., Goh, R.S.M.: Few-shot domain adaptation with polymorphic transformers. In: International Conference on Medical Image Computing and Computer-Assisted Intervention, Springer (2021) 330–340
- [31] Orlando, J.I., Fu, H., Breda, J.B., van Keer, K., Bathula, D.R., Diaz-Pinto, A., Fang, R., Heng, P.A., Kim, J., Lee, J., et al.: Refuge challenge: A unified framework for evaluating automated methods for glaucoma assessment from fundus photographs. *Medical image analysis* **59** (2020) 101570
- [32] Fumero, F., Alayón, S., Sanchez, J.L., Sigut, J., Gonzalez-Hernandez, M.: Rim-one: An open retinal image database for optic nerve evaluation. In: 2011 24th international symposium on computer-based medical systems (CBMS), IEEE (2011) 1–6
- [33] Bernal, J., Tajkbaksh, N., Sanchez, F.J., Matuszewski, B.J., Chen, H., Yu, L., Angermann, Q., Romain, O., Rustad, B., Balasingham, I., et al.: Comparative validation of polyp detection methods in video colonoscopy: results from the miccai 2015 endoscopic vision challenge. *IEEE transactions on medical imaging* **36** (2017) 1231–1249
- [34] Pogorelov, K., Randel, K.R., Griwodz, C., Eskeland, S.L., de Lange, T., Johansen, D., Spampinato, C., Dang-Nguyen, D.T., Lux, M., Schmidt, P.T., et al.: Kvasir: A multi-class image dataset for computer aided gastrointestinal disease detection. In: Proceedings of the 8th ACM on Multimedia Systems Conference. (2017) 164–169
- [35] Fan, D.P., Ji, G.P., Zhou, T., Chen, G., Fu, H., Shen, J., Shao, L.: Pranel: Parallel reverse attention network for polyp segmentation. In: International conference on medical image computing and computer-assisted intervention, Springer (2020) 263–273
- [36] Ganin, Y., Lempitsky, V.: Unsupervised domain adaptation by backpropagation. In: International conference on machine learning, PMLR (2015) 1180–1189
- [37] Tzeng, E., Hoffman, J., Saenko, K., Darrell, T.: Adversarial discriminative domain adaptation. In: Proceedings of the IEEE conference on computer vision and pattern recognition. (2017) 7167–7176
- [38] Dong, N., Kampffmeyer, M., Liang, X., Wang, Z., Dai, W., Xing, E.: Unsupervised domain adaptation for automatic estimation of cardiothoracic ratio. In: International conference on medical image computing and computer-assisted intervention, Springer (2018) 544–552

- [39] Wang, S., Yu, L., Yang, X., Fu, C.W., Heng, P.A.: Patch-based output space adversarial learning for joint optic disc and cup segmentation. *IEEE transactions on medical imaging* **38** (2019) 2485–2495